Loss of the Na(+)/H(+) exchanger NHE8 causes male infertility in mice by disrupting acrosome formation

Oberheide, K. and Puchkov, D. and Jentsch, T.J.

Journal of Biological Chemistry
2017 JUN 30 ; 292(26): 10845-10854
Doi: 10.1074/jbc.M117.784108

Publisher: American Society for Biochemistry and Molecular Biology

Loss of the Na^+/H^+ exchanger NHE8 causes male infertility in mice by disrupting acrosome formation

Received for publication, March 1, 2017, and in revised form, May 4, 2017 Published, Papers in Press, May 5, 2017, DOI 10.1074/jbc.M117.784108

Karina Oberheide[‡§], **Dmytro Puchkov**[‡], **and Thomas J. Jentsch**[‡§1]

From the [‡]*Leibniz-Forschungsinstitut für Molekulare Pharmakologie, D-13125 Berlin and* [§]*Max-Delbrück-Centrum für Molekulare Medizin, D-13125 Berlin, Germany*

Edited by Thomas Söllner

Mammalian sperm feature a specialized secretory organelle on the anterior part of the sperm nucleus, the acrosome, which is essential for male fertility. It is formed by a fusion of Golgi-derived vesicles. We show here that the predominantly Golgi-resident Na^+/H^+ exchanger NHE8 localizes to the developing acrosome of spermatids. Similar to wild-type mice, *Nhe8*$^{-/-}$ mice generated Golgi-derived vesicles positive for acrosomal markers and attached to nuclei, but these vesicles failed to form large acrosomal granules and the acrosomal cap. Spermatozoa from *Nhe8*$^{-/-}$ mice completely lacked acrosomes, were round-headed, exhibited abnormal mitochondrial distribution, and displayed decreased motility, resulting in selective male infertility. Of note, similar features are also found in globozoospermia, one of the causes of male infertility in humans. Germ cell-specific, but not Sertoli cell-specific *Nhe8* disruption recapitulated the globozoospermia phenotype, demonstrating that NHE8's role in spermiogenesis is germ cell-intrinsic. Our work has uncovered a crucial role of NHE8 in acrosome biogenesis and suggests that some forms of human globozoospermia might be caused by a loss of function of this Na^+/H^+ exchanger. It points to *NHE8* as a candidate gene for human globozoospermia and a possible drug target for male contraception.

Spermatogenesis is the process in which spermatozoa, the male gametes, are produced. After cycles of mitosis and meiosis, the haploid spermatids undergo drastic morphological changes to transform from a spherical cell into a polarized, elongated spermatozoon in a process called spermiogenesis (1). In this process, a large, mainly Golgi-derived membrane-enclosed structure, the acrosome, is formed on the anterior part of the sperm head. The acrosome plays a crucial role during fertilization. Mice and men in which all spermatozoa lack acrosomes are infertile (2, 3).

The Na^+/H^+ exchanger (NHE)[2] NHE8 is an integral membrane protein with 12 transmembrane domains as suggested by structures of bacterial homologues (4). NHE8 (SLC9A8) belongs to the *SLC9A* gene family that comprises nine members in mammals (5). These can be divided into two subfamilies: a plasma membrane subfamily including NHE1–5 and an organellar subfamily comprising NHE6–9. Plasma membrane NHEs are involved in the absorption of salt and water in epithelia and in regulating cytoplasmic pH, osmolarity, and cell volume. Knock-out mouse models have implicated these transporters in disorders like epilepsy and seizures, diarrhea, or metabolic acidosis (6–9). Organellar NHEs may regulate luminal ion concentrations, in particular the pH, of organelles in the secretory and endocytic pathways. These organelles display distinct, mostly acidic, luminal pH, which is crucial for organellar function (10–12). The specific pH of each organelle is determined by a balance of V-ATPase-mediated proton pumping and a "proton leak" pathway (13–15). Several studies in yeast (16) and mammalian cells (14, 15, 17–19) demonstrated that overexpression or knockdown of organellar NHEs leads to alkalinization or acidification of the organellar lumen, respectively, suggesting that these transporters provide a proton leak. The importance of organellar NHEs is underscored by mutations in *NHE6* and *NHE9* that lead to neurological disorders such as autism and epilepsy in humans (20, 21).

NHE8 (SLC9A8) is widely expressed in murine tissue, with high mRNA levels found in kidney, liver, skeletal muscle, and testes (17, 22). NHE8 localizes predominantly to mid- to trans-Golgi stacks, where it may alkalinize the luminal pH (17). NHE8 was also reported to be present on multivesicular bodies (23) and somewhat surprisingly at the apical brush-border membrane of epithelial cells of the intestine and renal proximal tubules (22, 24, 25). *Nhe8*$^{-/-}$ mice show impaired colonic mucin synthesis and bicarbonate secretion (26, 27), a dysfunction of the retinal pigment epithelium (28, 29), and male infertility (28, 30). In addition to NHE8, two other NHEs are known to affect male fertility in mice. Loss of plasma membrane NHE3 (SLC9A3) leads to increased fluid volume in the epididymis, thereby diminishing sperm concentration (31). Loss of the so-called sperm NHE (sNHE, a member (SLC9C1) of the *SLC9C* gene family) drastically reduces sperm motility and causes male infertility (32). sNHE, which contains additional voltage-sensor and nucleotide binding domains, localizes to the flagellum of mouse spermatozoa, where it may participate in a signaling complex at the plasma membrane (33).

Here we analyzed the role of NHE8 in male reproductive function. Mice lacking NHE8 globally or specifically only in

This work was supported, in part, by Deutsche Forschungsgemeinschaft Grant SFB 740, TP C05 (to T. J. J.) and by the European Research Council (FP7 2007-2013) ERC-Advanced Grant 294435 'CYTOVOLION' (to T. J. J.). The authors declare that they have no conflicts of interest with the contents of this article.

[1] To whom correspondence should be addressed: Robert-Rössle-Strasse 10, D-13125 Berlin, Germany. Fax: 49-30-9406-2960; E-mail: Jentsch@fmp-berlin.de.

[2] The abbreviations used are: NHE, Na^+/H^+ exchanger; GDV, Golgi-derived vesicle, WT, wild-type; PNA, peanut agglutinin; TEM, transmission electron microscope; PFA, paraformaldehyde

germ cells produced round-headed spermatozoa lacking the acrosomal cap. This resembles human globozoospermia which likewise is associated with infertility. Instead of acrosomes, *Nhe8*$^{-/-}$ spermatids displayed isolated, sometimes nucleus-attached Golgi-derived vesicles (GDVs). Hence NHE8 may play a crucial role in the fusion of GDVs to form acrosomes. Our work suggests *NHE8* as a candidate gene for human globozoospermia and as a possible drug target for male contraception.

Results

Disruption of Nhe8 causes male infertility in mice

We established *Nhe8*$^{-/-}$ mice (Fig. 1*A*) to elucidate physiological roles of NHE8. Wild-type (WT), *Nhe8*$^{+/-}$, and *Nhe8*$^{-/-}$ mice were born at Mendelian ratio (Fig. 1*H*), grew normally, and all littermates were superficially indistinguishable. Complete loss of NHE8 protein in *Nhe8*$^{-/-}$ mice was confirmed in several organs by immunoblot analysis which in the WT showed NHE8 signals of ~60 and 85 kDa as reported (22) (Fig. 1*B*). NHE8 expression was prominent in kidney, testes, and epididymis, but very low in the female reproductive system (Fig. 1*B*). Although we frequently obtained offspring from *Nhe8*$^{-/-}$ females, male *Nhe8*$^{-/-}$ mice never produced progeny, as reported previously (26, 30). Vaginal plugs observed in breedings with male *Nhe8*$^{-/-}$ mice indicated normal mating behavior, libido, copulation, and ejaculation. Body (WT, 27.5 ± 1.5 g; *Nhe8*$^{-/-}$, 26.4 ± 1.0 g; $n = 12$) and testes weight (WT, 0.57 ± 0.03% of body weight; *Nhe8*$^{-/-}$, 0.59 ± 0.04% of body weight; $n = 12$) was unchanged in *Nhe8*$^{-/-}$ mice. Their male reproductive systems appeared macroscopically normal (Fig. 1*C*), as did their seminiferous tubules (Fig. 1*E*), the diameters of which were unchanged (Fig. 1*I*).

Nhe8$^{-/-}$ *mice have round-headed spermatozoa and lack acrosomes*

Seminiferous tubules of both WT and *Nhe8*$^{-/-}$ mice contained spermatozoa (Fig. 1*F*) and the epididymal sperm concentration was not significantly different (Fig. 1*J*). Contrasting with the typical elongated heads of WT spermatozoa (Fig. 1*G*, *top*), *Nhe8*$^{-/-}$ spermatozoa had round heads, within seminiferous tubules (Fig. 1*G*, bottom) or the cauda epididymis (Fig. 1*D*). Their motility was drastically reduced (Fig. 1*K*). *Nhe8*$^{-/-}$ spermatozoa lacked acrosomes and showed an abnormal distribution of mitochondria which were found in sperm heads instead of forming a sheath around the initial part of the flagellum. This was revealed by crosses with "green sperm" mice (34) that express dsRed in mitochondria and GFP in acrosomes (Fig. 2*A*) and by labeling acrosomes with peanut agglutinin (PNA) (35) and mitochondria with MitoTracker® (Fig. 2*B*) and ascertained by transmission electron microscopic (TEM) images (Fig. 3, *A*–*D*). Because the mitochondrial sheath provides ATP for flagellar movement (36), this finding might explain the reduced motility of *Nhe8*$^{-/-}$ spermatozoa.

The lack of Golgi-derived acrosomes upon ablation of the Golgi-resident NHE8 protein (17) points to a germ cell-intrinsic effect, but also defects in germ-cell nurturing Sertoli cells or hormone-producing Leydig cells may cause infertility (37). X-Gal staining of testes from mice carrying the *lacZ* reporter gene in the *Nhe8* locus (Fig. 1*A*) revealed *Nhe8* transcription in seminiferous tubules, but not in intertubular Leydig cells (Fig. 2*C*). Immunofluorescence detected NHE8 protein in WT (but not *Nhe8*$^{-/-}$) germ cells, where it localized to an acrosome-like structure in close proximity to the nucleus (Fig. 2*D*). NHE8 perfectly co-localized with the acrosomal marker PNA in all four phases of spermiogenesis (Fig. 2*E*). Absence of immunoreactivity in *Nhe8*$^{-/-}$ testes (Fig. 2*D*) confirmed the specificity of labeling of preacrosomal granules. However, it cannot strictly guarantee that NHE8 is expressed on mature acrosomes because these structures are not present in *Nhe8*$^{-/-}$ testes. Comparison of spermiogenesis between the genotypes showed that only the Golgi phase appeared normal in *Nhe8*$^{-/-}$ mice (Fig. 2*F*). Instead of a single acrosomal granule that grows and flattens in WT mice, many small PNA-positive vesicles were detected on the nuclear surface in *Nhe8*$^{-/-}$ spermatids (Fig. 2*F*, *cap phase*). In the maturation phase, the resulting acrosomeless *Nhe8*$^{-/-}$ spermatids failed to obtain the typical elongated shape, although nuclei were condensed (Fig. 2*F*, *maturation phase*). TEM of WT testis showed the generation of acrosomal granules by fusion of GDVs, their attachment to the nucleus (Fig. 3*E*), growth, and flattening (Fig. 3*F*), as well as nuclear elongation (Fig. 3*G*). By contrast, in *Nhe8*$^{-/-}$ mice GDVs accumulated in the region between the Golgi and the nucleus (Fig. 3, *H* and *I*) but failed to generate larger granules or acrosomal caps. GDVs were more electron-dense in *Nhe8*$^{-/-}$ cells. Although spermatozoa in the seminiferous tubules of *Nhe8*$^{-/-}$ mice had condensed chromatin, their nuclei frequently displayed irregular shapes (Fig. 3*J*). The preacrosomal granule is attached to the nucleus by a cytoskeletal scaffold, the acroplaxome (38). The acroplaxome was visible in TEM as a dense plate in the subacrosomal space in WT spermatids (Fig. 3*K*) as well as in the space between the nucleus and the GDVs in *Nhe8*$^{-/-}$ spermatids (Fig. 3, *L* and *M*). This indicates that the defects in acrosome biogenesis are probably caused by impaired fusion of GDVs, whereas tethering of these vesicles to the nuclear envelope seems to be unaffected.

Germ cell-specific disruption of Nhe8 causes a phenotype indistinguishable from Nhe8$^{-/-}$ *mice*

Our data suggest that NHE8 is directly involved in acrosome biogenesis and that disruption of this process causes the infertility of *Nhe8*$^{-/-}$ mice. To test this hypothesis, *Nhe8* was specifically deleted in Sertoli or germ cells by crossing *Nhe8*$^{lox/lox}$ mice with AMH-Cre (39) and Stra8-iCre (40) mice, respectively. Specificity of Cre expression was ascertained by crosses with R26R reporter mice (41) (Figs. 4*A* and 5*A*). In the following, we refer to the resulting Sertoli cell- and germ cell-specific knock-out mice as SC-ΔNHE8 and GC-ΔNHE8 mice, respectively. NHE8 protein levels of SC-ΔNHE8 testes were indistinguishable from WT mice, indicating that NHE8 is not, or is only at very low levels, expressed in Sertoli cells (Fig. 4*B*). As expected, male SC-ΔNHE8 mice were fertile and always produced offspring when mated over a 2-month period ($n = 7$ SC-ΔNHE8 males). Neither morphology and diameter of seminiferous tubules (Fig. 4, *C* and *E*), nor sperm morphology was affected (Fig. 4, *E* and *F*). Spermatozoa from SC-ΔNHE8 mice displayed normal acrosomal caps and mitochondrial sheaths (Fig. 4*G*). Hence NHE8 is dispensable in Sertoli cells for normal

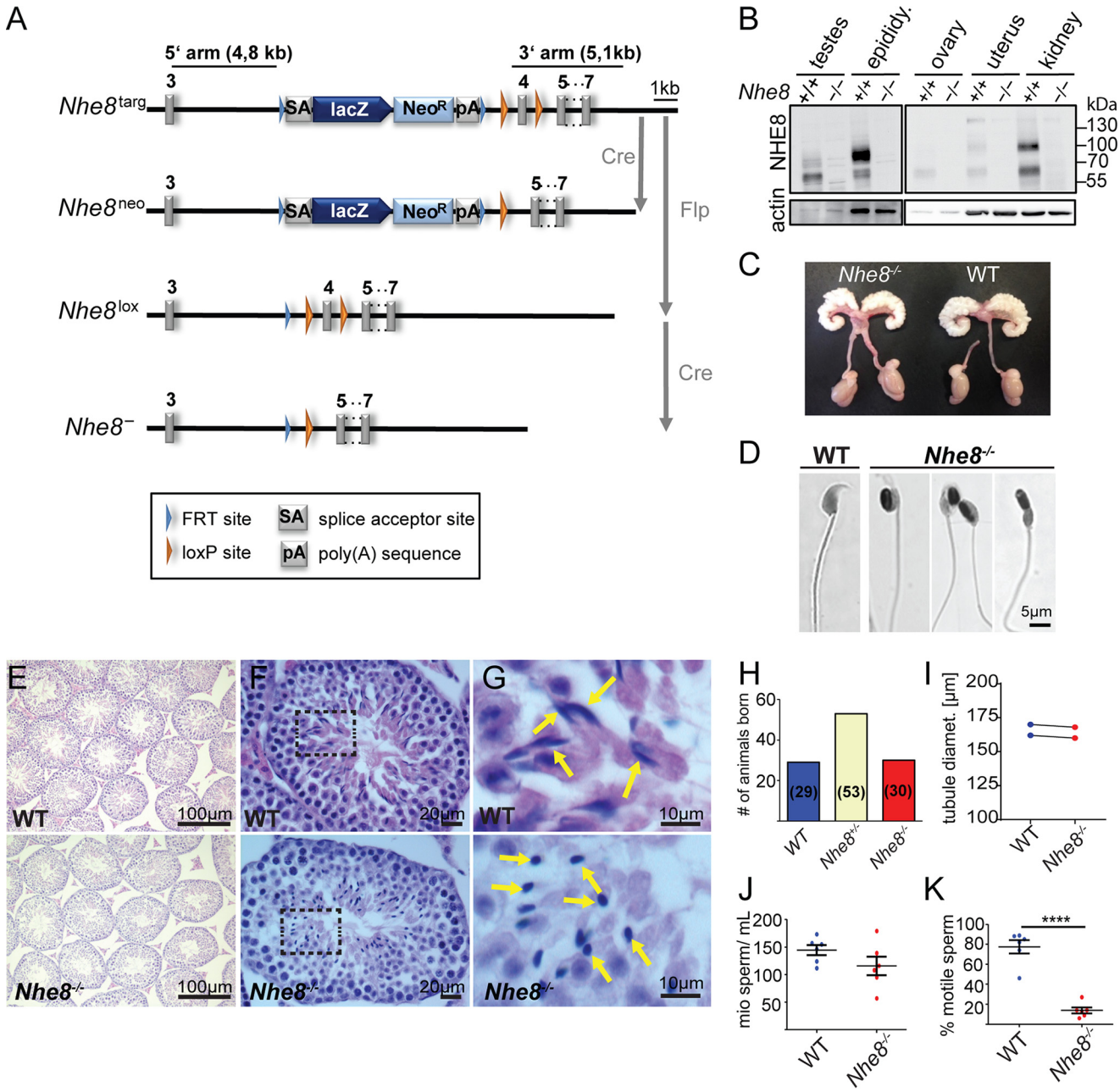

Figure 1. The male reproductive system and spermatozoa in WT and *Nhe8*$^{-/-}$ mice are shown. *A*, *Nhe8* targeting strategy. Targeted *Nhe8* allele (*Nhe8*^{targ}): a cassette comprising a splice acceptor site (*SA*), the *lacZ* gene, the neomycin resistance gene (*Neo*^{R}), and a sequence encoding a poly(A) tail is flanked by FRT sites (*blue triangles*). Exon 4 is flanked by loxP sites (*orange triangles*). Mating to Cre recombinase expressing deleter mice will lead to excision of exon 4, but not the cassette upstream of the loxP site. This allele (*Nhe8*^{neo}) can be used for transcription analysis of *Nhe8* by making use of the *lacZ* reporter gene. The floxed allele (*Nhe8*^{lox}) was obtained by mating *Nhe8*^{targ} mice to FLPe recombinase-expressing deleter mice. Subsequent mating to Cre recombinase expressing deleter mice will result in the null allele (*Nhe8*$^{-/-}$). *B*, Western blot analysis of NHE8 expression in the male and female reproductive system and kidney of 4-month-old WT and Nhe8$^{-/-}$ mice. Protein load, 20 μg per lane; antibody, rbαNHE8-CT. *C*, macroscopic morphology of the male reproductive system. *D*, hematoxylin and eosin (H&E) staining on spermatozoa isolated from the caudae epididymides of WT and *Nhe8*$^{-/-}$ mice. *E*, H&E staining of paraffin sections of testes from 11-week-old WT and *Nhe8*$^{-/-}$ mice. *F*, H&E staining of paraffin sections of the testis. Spermatozoa were found in the luminal region of the seminiferous tubules in both WT and *Nhe8*$^{-/-}$ mice. *G*, magnification of the areas delineated by *broken lines* in *F* to show details of sperm heads (indicated by *yellow arrows*). *H*, WT, *Nhe8*$^{+/-}$, and *Nhe8*$^{-/-}$ mice are born at Mendelian ratio (29:53:30). *I*, unchanged tubule diameter in *Nhe8*$^{-/-}$ mice (mean WT, 166 $\pm$ 4 μm, n = 332 tubules of two mice; mean *Nhe8*$^{-/-}$, 164 $\pm$ 4 μm, n = 328 tubules of two mice). Connected dots are littermates. *J*, sperm concentration in the caudae epididymides (mean WT, 144.6 $\pm$ 9.3 million sperm/ml; mean *Nhe8*$^{-/-}$, 115.8 $\pm$ 16.8 million sperm/ml; 6 mice; $p < 0.17$ unpaired Student's t test). *K*, drastically reduced motility of spermatozoa from *Nhe8*$^{-/-}$ mice (mean WT, 77.3 $\pm$ 6.6% motile sperm; mean *Nhe8*$^{-/-}$, 13.8 $\pm$ 2.9% motile sperm; 6 mice per genotype; ****, $p < 0.0001$, unpaired Student's t test).

sperm development and fertility. In contrast, testicular NHE8 protein levels were drastically reduced in GC-ΔNHE8 mice (Fig. 4*B*), indicating that in mouse testes NHE8 is predominantly expressed in germ cells. The testicular phenotype of GC-ΔNHE8 mice appeared identical to that of *Nhe8*$^{-/-}$, except for the finding that ~5% of spermatozoa from GC-ΔNHE8 mice appeared normal, which can be attributed to the known ~95% deletion efficiency of Stra8-iCre mice (40). The identical phenotype included male infertility (n = 15 GC-ΔNHE8 males), normal morphology and diameter of the seminiferous

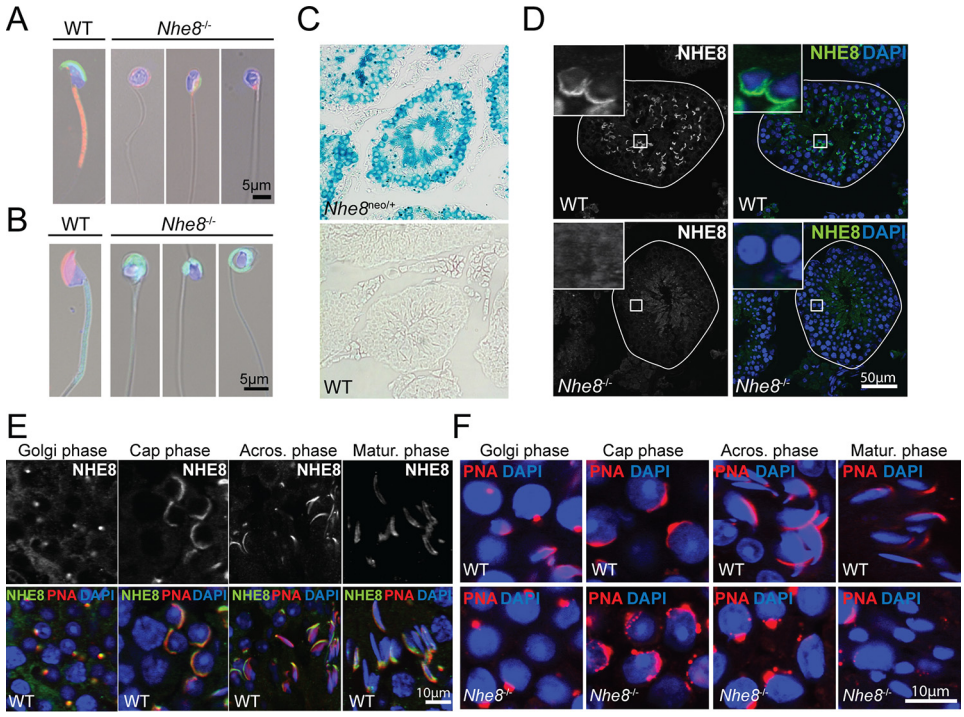

Figure 2. NHE8 expression in testes and germ cells is shown. *A*, mature green spermatozoa (expressing GFP tagged acrosin (*in green*) and dsRed tagged mitochondria (*in red*) isolated from the caudae epididymides of WT and $Nhe8^{-/-}$ green sperm mice, fixed and counterstained with αGFP (*green*), αdsRed (*red*), and DAPI (*blue*) to reveal nuclei. *B*, immunofluorescent labeling of isolated WT and $Nhe8^{-/-}$ spermatozoa. Labeling of the acrosomal cap (PNA, *red*), the nucleus (DAPI, *blue*), and the mitochondrial sheath (MitoTracker®, *green*). *C*, X-Gal staining on sections of $Nhe8^{neo/+}$ or WT testes showing Nhe8 expression in *blue*. *D*, immunofluorescent labeling of NHE8 in seminiferous tubules (surrounded by *white lines*) of testis from WT and $Nhe8^{-/-}$ mice. *Magnified regions* show the caplike NHE8-positive structures in the WT. Antibody, rbαNHE8–10. *E*, co-localization of NHE8 (*green*) with the acrosomal marker PNA (*red*) to the developing acrosome in all four phases of spermiogenesis in WT mice. Antibody, rbαNHE8–10. Nuclei labeled with DAPI. *F*, PNA labeling (*red*) contrasts the normal development of the nucleus-apposed acrosome in WT mice to the impaired biogenesis in $Nhe8^{-/-}$ mice. Results shown in this figure were observed in at least two WT/KO mouse pairs.

tubules (Figs. 4*C* and 5*C*), and the presence of round-headed sperm (Fig. 5, *C* and *D*) lacking both acrosomes and mitochondrial sheaths (Fig. 5*E*). Acrosome biogenesis was similarly affected in global and germ cell-specific $Nhe8^{-/-}$ mice (Fig. 5*F* and Fig. 6, *A*–*F*). The only ~95% deletion efficiency of Stra8-iCre mice allowed us to directly compare WT and NHE8-deficient cells side by side in sections from GC-ΔNHE8 mice. NHE8-positive cells displayed acrosomal caps and elongated nuclei (Fig. 6, *G* and *H*, *yellow arrows*), whereas NHE8-deficient cells in the same tubule lacked acrosomes and had round nuclei. We conclude that NHE8 is required in germ cells for intact acrosome biogenesis, sperm development, and male fertility.

Discussion

Spermatogenesis is the long process that leads from diploid spermatogonia to spermatozoa, highly differentiated haploid motile gametes. The complexity of this differentiation process implies that mutations in many different genes can interfere with spermatogenesis and thereby result in infertility (3). We now showed that disruption of *Nhe8* causes a specific infertility syndrome, globozoospermia, which is characterized by round-headed, acrosome-less sperm (42, 43). The acrosome is a unique secretory sperm organelle that is essential for male fertility (2, 3). Golgi-resident NHE8 was needed in a cell-intrinsic manner for the biogenesis of this Golgi-derived organelle. Our work adds NHE8 to the growing list of intracellular ion transport proteins with crucial roles in vesicle trafficking and fusion (44).

Acrosomes are unique large vesicles sandwiched between the plasma membrane and the nucleus at the tip of sperm cells. The acrosome reaction, a highly unusual form of exocytosis, releases lytic enzymes and exposes acrosomal membrane proteins at the outer sperm membrane (3, 45). The release of lytic enzymes is thought to facilitate the dispersion of cumulus cells and the penetration of the zona pellucida, but KO mice showed that many of these enzymes are individually dispensable for fertility (1, 3). By contrast, the immunoglobulin family member Izumo, an acrosome-resident membrane protein that is exposed at the sperm surface after the acrosome reaction, is absolutely required for sperm-oocyte fusion and hence fertility (3, 46). Acrosomes may also play a role in shaping sperm nuclei by their acroplaxome-mediated tight interaction (38). Indeed, the loss of the acrosome is generally associated with abnormally shaped nuclei in globozoospermia (45, 47–49). The loss of a mitochondrial sheath, as observed here, is also found in other genetic forms of globozoospermia (47–49) but the underlying mechanism is unclear.

Acrosomes are mainly generated by fusion of Golgi-derived vesicles but they share some properties, including their strongly acidic luminal pH and many degradative enzymes, with lysosomes (50, 51). The molecular mechanisms underlying the budding, trafficking, and fusion of GDVs are still largely unknown. We detected NHE8 not only on the Golgi, where it has been found in previous studies (17), but also during all phases of spermiogenesis on acrosomal granules and finally on mature

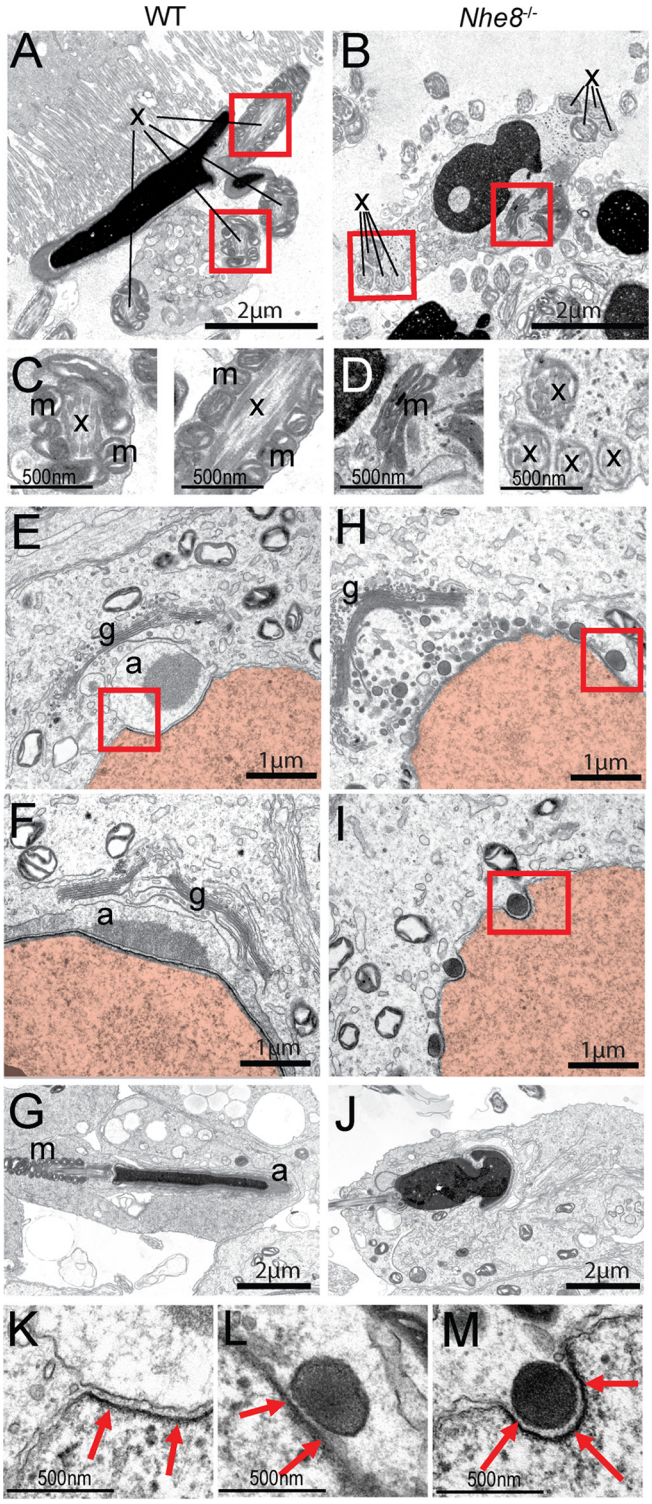

Figure 3. Defective formation of the acrosome and mitochondrial sheath in *Nhe8*$^{-/-}$ mice is shown. *A* and *B*, TEM images of epididymal spermatozoa from WT (*A*) and *Nhe8*$^{-/-}$ (*B*) mice. *x*: axoneme, *m*: mitochondria. *Red boxes* indicate areas of *A* and *B* that are shown in higher magnification in *C* and *D*, respectively. *E–G*, TEM images from WT mice showing different phases of spermiogenesis. *E*, Golgi phase. *F*, cap phase. *G*, maturation phase. *H–J*, equivalent images from *Nhe8*$^{-/-}$ mice. *H*, electron-dense vesicles attached to the nuclear envelop can be found. Acrosomal granules or acrosomal caps were not detected. *I*, single dense vesicles were found in nuclear notches. *J*, acrosome-less spermatozoa with irregularly shaped nuclei. *g*: Golgi apparatus; *a*: acrosome or acrosomal granule; *m*: mitochondrial sheath; *x*: cilia crossections. Nuclei highlighted in red. *K–M*, magnification of the areas delineated by *red lines* in *E*, *H*, and *I*, respectively, reveal the acroplaxome (*red arrows*).

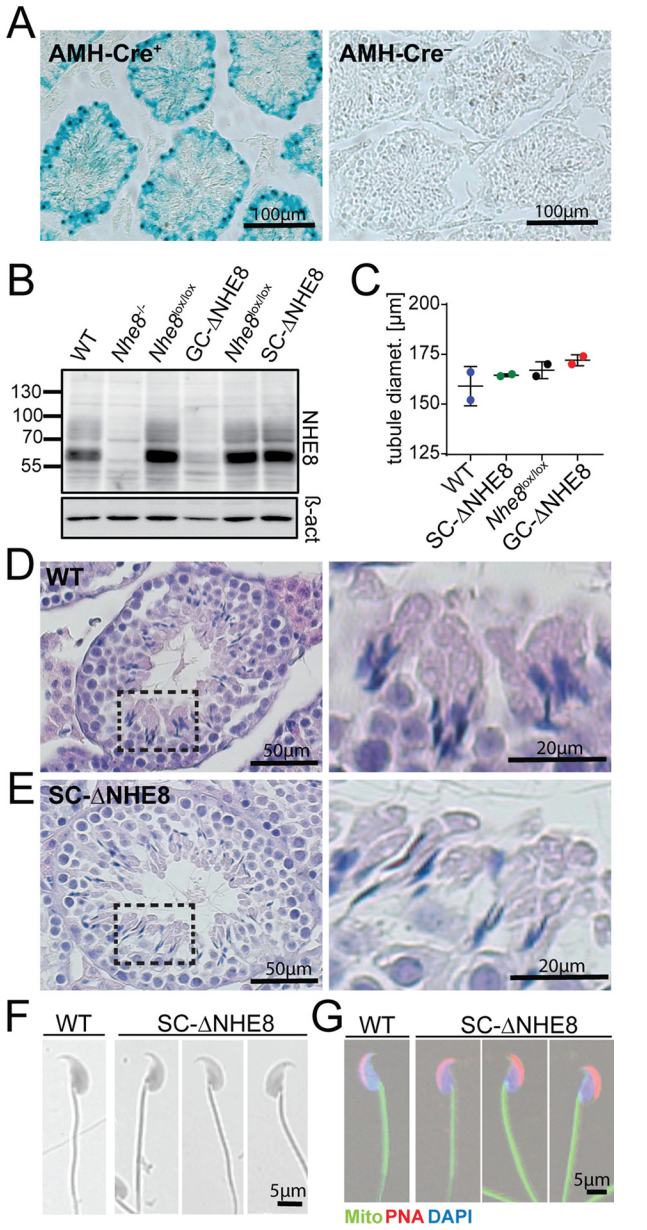

Figure 4. NHE8 is dispensable in Sertoli cells for normal spermiogenesis. *A*, X-gal staining on frozen tissue sections from Rosa26R$^{+/-}$, AMH-Cre^{+} mice, and control mice (Rosa26R$^{+/-}$; AMH-Cre^{-}). *B*, Western blots of testes lysates indicate complete absence of the NHE8 protein in *Nhe8*$^{-/-}$ mice (*lane 2*) and drastic reduction in GC-ΔNHE8 mice (*lane 4*) in which *Nhe8* is specifically deleted in germ cells using Stra8-iCre mice. Protein levels in *Nhe8*$^{lox/lox}$ or SC-ΔNHE8 mice are equal to *Nhe8*$^{+/+}$ mice. Protein load, 30 μg per lane. Antibody, rbαNHE8-CT. Actin served as loading control. *C*, tubule diameter was unchanged between genotypes (WT mean, 159 ± 7 μm, n = 51 tubules from two mice; SC-ΔNHE8 mean, 165 ± 0.5 μm, n = 90 tubules from two mice; *Nhe8*$^{lox/lox}$ mean, 167 ± 3 μm, n = 334 tubules from two mice; GC-ΔNHE8 mean, 172 ± 2 μm, n = 344 tubules from three mice). *D* and *E*, H&E staining on testes sections from (*D*) WT and (*E*) SC-ΔNHE8. *Right panels* show a magnification of the areas delineated by *broken lines*. *F*, H&E staining of isolated sperm from SC-ΔNHE8 mice. *G*, fluorescent labeling of the acrosome (PNA, *red*), nucleus (DAPI, *blue*), and mitochondrial sheath (MitoTracker®, *green*) on isolated spermatozoa of WT and SC-ΔNHE8 mice.

acrosomes. Together with the observation that sperm-specific *Nhe8* disruption sufficed to impair acrosome biogenesis, this localization strongly suggests that NHE8 is directly required for acrosome formation. As we observed GDVs in *Nhe8*$^{-/-}$ spermatids by both PNA labeling and electron microscopy, it is

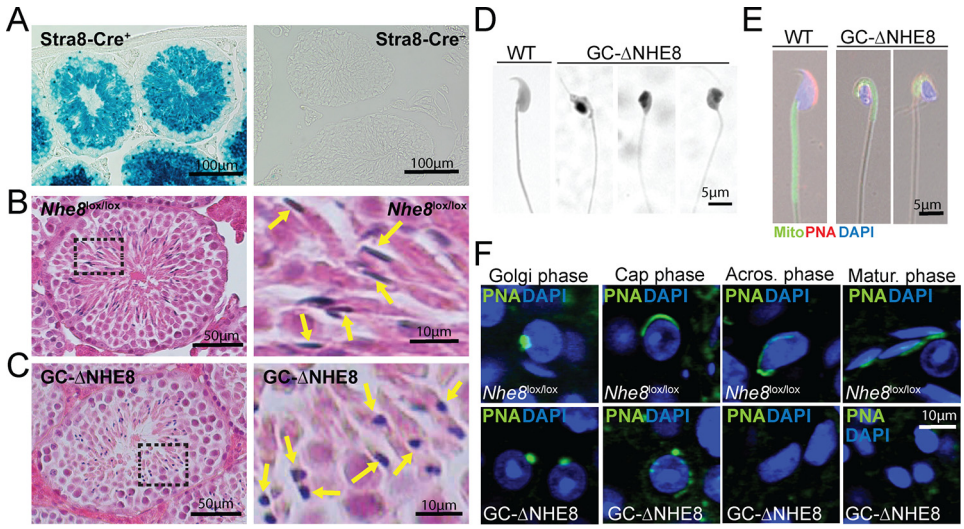

Figure 5. Germ cell-specific disruption of *Nhe8* leads to round-headed acrosome-less spermatozoa. *A*, X-gal staining on frozen tissue sections from Rosa26R$^{+/-}$, Stra8-Cre^{+} mice, and control mice (Rosa26R$^{+/-}$; Stra-Cre^{-}). *B* and *C*, H&E staining on testes sections from (*B*) *Nhe8*$^{lox/lox}$ and (*C*) GC-ΔNHE8 mice. *Right panels* show a magnification of the areas delineated by *broken lines*. Sperm heads indicated by *yellow arrows*. *D*, H&E staining of isolated sperm from WT and GC-ΔNHE8 mice. *E*, fluorescent labeling of the acrosomal cap (PNA, *red*), the crescent-shaped nucleus (DAPI, *blue*), and the mitochondrial sheath (Mito-Tracker®, *green*) on isolated spermatozoa of WT and GC-ΔNHE8 mice. *F*, PNA labeling (*green*) illustrating the normal development of the nucleus-apposed acrosome in *Nhe8*$^{lox/lox}$ mice in contrast to the impaired biogenesis in GC-ΔNHE8 mice.

highly likely that NHE8 is needed for its fusion to acrosomes rather than for the detachment from the Golgi. Indeed, NHE8 and the *Saccharomyces cerevisiae* orthologue Nhx1p, which is closely related to organellar NHEs, have been proposed as regulators of vesicle fusion (23, 52). *NHE8* knockdown in HeLa cells led to an increase of intraluminal vesicles in multivesicular bodies, suggesting NHE8 as a regulator of vesiculation or a promoter of the fusion of late multivesicular bodies with lysosomes (23). Finally *Hrb*$^{-/-}$, *Pick1*$^{-/-}$, and *GOPC*$^{-/-}$ mice, which display globozoospermia very similar to *Nhe8*$^{-/-}$ mice, are thought to result from defective GDV fusion (47–49).

How might NHE8 influence the fusion of GDVs? Being a Na^+/H^+-exchanger, its loss may change both vesicular pH and Na^+ concentration. These changes can secondarily affect other luminal ion concentrations like that of Ca^{2+}, the release of which may be needed for vesicle fusion and trafficking (53–55). Although not quite reaching the pH of lysosomes, the luminal pH of acrosomes (pH ~5.3) (56, 57) is more acidic than that of the Golgi (estimated pH ~5.9–6.3, depending on cell type) (58–60). A proton "leak" by NHE8 might tune the acidification of GDVs. Luminal pH can affect vesicular transport *e.g.* in the endosomal/lysosomal pathway (61), where it may affect endosomal carrier formation (62) and the cytosolic binding of proteins involved in trafficking (63). Alternatively or additionally, NHE8 might directly interact with proteins of the fusion machinery, as shown for GOPC and Pick1 (47). Both proteins possess a PDZ domain whereas NHE8 features a PDZ-binding domain. However, preliminary co-immunoprecipitation experiments (data not shown) failed to ascertain the attractive hypothesis that NHE8 binds to one of these proteins.

Although we unambiguously identified a germ cell-intrinsic defect in acrosome formation as underlying the male infertility of *Nhe8*$^{-/-}$ mice, Xu *et al.* (30) recently suggested that it is caused by reduced testosterone levels stemming from impaired trafficking of the luteinizing hormone receptor in Leydig cells. The authors state that NHE8 is mainly expressed in Leydig cells (30), without, however, using *Nhe8*$^{-/-}$ controls as done here. Disconcertingly, they also observed smaller testes and azoospermia. We cannot explain this discrepancy, but differences in genetic background or the disruption of an additional gene in their gene trap approach (30) might possibly be invoked.

The ablation of several genes causes globozoospermia in mice, but so far only three genes are known to underlie globozoospermia in humans, *DPY19L2*, *SPATA16,* and *PICK1* (64–66). Genetic causes remain unknown in one-third of globozoospermia patients. This study adds *SLC9A8* to the list of candidate genes for this disorder. Moreover, it expands the list of ion transporters involved in vesicle trafficking or fusion and highlights the biological importance of vesicular ion homeostasis.

Experimental procedures

Mice

Animal care and experiments conformed to German animal protection laws and were approved by the Berlin authorities (Landesamt fr Gesundheit und Soziales Berlin). Sperm of mice heterozygous for the targeted *Nhe8*^{targ} allele (*Slc9a8*$^{tm1a(KOMP)Wtsi}$) was ordered via the Knockout Mouse Project (KOMP) (Davis, CA). *In vitro* fertilization of C57BL/6 female mice was carried out by the transgenic core facility of the Max-Delbrück-Centrum für Molekulare Medizin (MDC) Berlin. Targeted mice were crossed to Cre or FLPe recombinase expressing deleter mice to generate different *Nhe8* mouse lines (see Fig. 1*A*) (67, 68). *Nhe8*$^{lox/lox}$ mice were crossed to AMH-Cre mice (B6-Tg(Amh-cre)8815Reb/J, obtained from The National Institute for Agronomic Research) or Stra8-iCre mice (B6.FVB-Tg (Stra8-iCre)1Reb/LguJ, obtained from The Jackson Laboratory, no. 017490) for cell-specific deletion of *Nhe8* in Sertoli cells or male premeiotic germ cells, respectively (39, 40). AMH-Cre

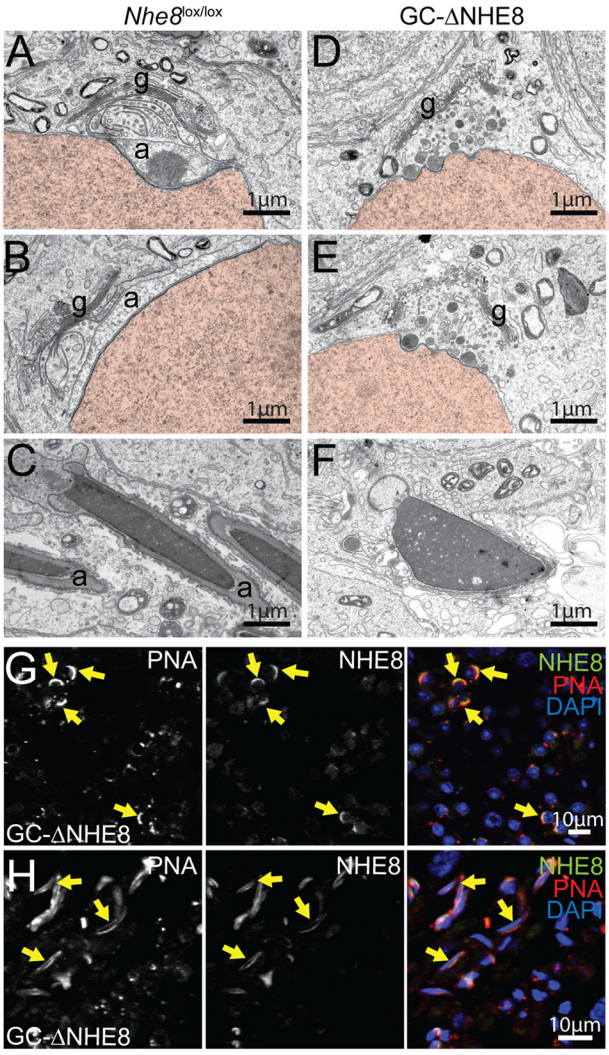

Figure 6. Defective acrosome biogenesis in GC-ΔNHE8 mice is shown. *A–C*, TEM images from *Nhe8*$^{lox/lox}$ mice representing the (*A*) Golgi, (*B*) cap, or (*C*) maturation phase of spermiogenesis. *D–F*, TEM images from GC-ΔNHE8 mice. *D and E*, electron-dense vesicles accumulate between the Golgi and the nuclear envelope, but acrosomal granules or acrosomal caps were not found. *F*, in mature spermatozoa, DNA is condensed, but sperm heads are not elongated and lack acrosomal caps. *g*, Golgi apparatus; *a*, acrosome. Nuclei are in *red*. *G*, remaining NHE8 signal in GC-ΔNHE8 mice co-localizes with the acrosome in the cap phase of spermiogenesis (indicated by *yellow arrows*). Spermatids lacking NHE8 lack acrosomes, having instead PNA-positive vesicles attached to their nucleus. *H*, besides the round-headed, acrosome-less spermatozoa, spermatozoa with intact acrosomes and elongated nuclei can be found in some tubules in GC-ΔNHE8 mice. These spermatozoa express NHE8 (indicated by *yellow arrows*).

mice and Stra8-iCre mice were crossed to Rosa26R Cre reporter mice (B6.129-Rosa26tm, obtained from Fred Hutchinson Research Center). Green sperm mice (34) were obtained from RIKEN (B6D2-Tg(CAG/Su9-DsRed2,Acr3-EGFP) RBGS002Osb, no. RBRC03743) and crossed to *Nhe8*$^{+/-}$ mice.

Generation of NHE8 antibodies

Antibodies to two epitopes of NHE8 (^{494}NAIESEHLSELTEEEYEAH^{512} for rbαNHE8–10 and ^{559}EEVRQGPSGSEDDEQELF^{576} for rbHE8-CT) were raised in rabbits (Pineda Antikörper-Service) and affinity-purified. *Nhe8*$^{-/-}$ tissue served as a control.

Immunohistochemistry

Mice were anesthetized and perfused with PBS, followed by 1% (w/v) paraformaldehyde (PFA) in PBS. Testes were postfixed in 1% PFA (1 h), transferred to 30% (w/v) sucrose (24–48 h) and embedded in Tissue-Tek® O.C.T. compound (Sakura). 8- to 10-μm frozen sections were cut with a Cool-Cut microtome (Microm HM 560, Cryostat-Series, Thermo Scientific). For immunofluorescent labeling, sections were postfixed with 1% PFA, incubated with 30 mM glycine, permeabilized using 0.2% Triton X-100 and incubated with primary NHE8 antibody (1:100) in 3% BSA in PBS supplemented with 0.1% Triton X-100 at 4 °C overnight. Secondary antibodies were coupled to Alexa fluorophores (1:1000) (Molecular Probes) and counterstained with DAPI (1:10000) (Invitrogen) for 45–60 min at room temperature in the dark. Peanut agglutinin coupled to Alexa fluorophores was used as an acrosomal marker and applied together with secondary antibodies (1:800) (Molecular Probes). Confocal images were taken with a Zeiss LSM 510 META laser scanning microscope and ZEN software (Zeiss). Image processing was done using ZEN software (Zeiss). All stainings were repeated in at least three independent experiments. Spermatids were assigned to different phases of spermiogenesis by their location inside the seminiferous tubule (cells move toward the luminal region during the maturation process) and nuclear morphology. In WT mice, the size and form of the acrosomal cap served as another indicator to assign the correct phase of spermiogenesis.

Histology

For histological analyses, mice were perfused with 4% PFA/PBS (w/v) and organs were postfixed overnight at 4 °C. After dehydration in a graded ethanol series, organs were stored in isopropanol/paraffin overnight at 65 °C. After incubation in 100% paraffin for another 6–10 h, organs were embedded in paraffin and 6-μm sections were cut (Cool-cut Microm HM 355 S, Thermo Scientific). Hematoxylin and eosin staining was performed on these sections or on isolated epididymal sperm dried on coverslips. X-Gal staining was done on frozen sections from *Nhe8*$^{neo/+}$ or *Nhe8*$^{+/+}$ mice (see "Immunohistochemistry") for 12–48 h at 37 °C in a humidified chamber (staining solution: 2 mM $MgCl_2$, 5 mM $K_3Fe(CN)_6$, 5 mM $K_4Fe(CN)_6$, 0.2% Nonidet P-40, 0.1% sodium deoxycholate, 1 mg/ml X-Gal in 0.1 M phosphate buffer, pH 7.4). Images of X-Gal stainings and hematoxylin and eosin stainings were taken with an AxioCam MRa5 (Zeiss) on an Axiophot microscope (Zeiss) with an Achrostigmat 5×/0.12, Plan-Neofluar 10×/0.30, or Plan-Neofluar 40×/0.75 objective using the ZEN software (Zeiss). Image processing was done with Adobe Photoshop.

Isolation and analysis of mouse spermatozoa

Mice were killed by cervical dislocation and the caudae epididymides were removed immediately. They were thoroughly cleaned of fat and blood vessels, each transferred to 200 μl of cryoprotective agent (CPA) (180 g/liter raffinose, 30 g/liter skim milk), and ruptured. Sperm was allowed to swim out for 5 min at room temperature. For stainings, sperm in cryoprotective agent were diluted in PBS and smeared on coverslips. Staining was performed as for immunohistochemistry. For investigation of

the mitochondrial sheath, spermatozoa were incubated with MitoTracker® green (Molecular Probes) at a final concentration of 100 nM for 10 min at 37 °C, centrifuged 1 min at 5000 × *g*, resuspended in PBS, and smeared on coverslips. Green sperm were stained with chαGFP (Aves Labs), mαdsRed (Clontech), and DAPI.

Sperm motility measurements

Isolated sperm were incubated in human tubal fluid (HTF) medium at 37 °C for 5 min in a 1:50 dilution. Sperm motility and concentration were assessed using IVOS sperm analyzer version 12 (Hamilton Thorne Research, Beverly, MA). Spermatozoa were tracked for 30 s and images were captured at a frequency of 60 Hz. The cutoff of motile spermatozoa was 20 μm/s for the path velocity (distance traveled along a smoothed path divided by elapsed time) and 30 μm/s for the linear velocity (straight-line distance between starting and end point divided by elapsed time).

Western blot analyses

Membrane fractions were isolated from mouse tissue. To this end, tissue homogenate was prepared in 20 mM Tris-HCl pH 7.4, 140 mM NaCl, 5 mM EDTA with protease inhibitors (4 mM Pefabloc®, cOmplete EDTA-free protease inhibitor mixture (Roche)) using a glass dounce homogenizer and cleared by centrifugation for 10 min at 1000 × *g* twice. Membrane fractions were pelleted from the cleared homogenate by ultracentrifugation for 30 min at 270,000 × *g*, and the pellet was resuspended by sonication in 50 mM Tris pH 6.8, 5 mM EDTA, 2% SDS (w/v) with protease inhibitors. Equal amounts of protein were separated by SDS-polyacrylamide gel electrophoresis and blotted onto nitrocellulose. Blots were reprobed with mouse anti-β-actin (clone AC-74; Sigma, no. A2228) (1:5000) as a loading control.

Transmission electron microscopy

Mice were anesthetized and perfused transcardially (4% formaldehyde, 2.5% glutaraldehyde in 0.1 M phosphate buffer). Testes were isolated and postfixed in the same solution overnight at 4 °C, embedded in 5% agar, and sliced (200 μm thick) with a vibratome. Slices were postfixed in 1% OsO4 and 1.5% potassium hexacyanoferrate, dehydrated in a methanol gradient and propylene oxide, and flat embedded in epoxy resin. After polymerization, seminiferous tubules were trimmed, sectioned ultrathin, and analyzed using a Zeiss 900 transmission electron microscope.

Statistics

Statistical significance was assessed using the paired or unpaired Student's *t* test (Prism, GraphPad Software). Errors are indicated as ± S.E.

Author contributions—K. O. designed, performed, and evaluated experiments and wrote the paper. D. P. designed, performed, and evaluated TEM experiments and wrote the paper. T. J. J. initiated the project, designed and evaluated experiments, and wrote the paper.

Acknowledgments—We thank K. Fuchs for technical assistance and the RIKEN BioResource Center for providing the "green sperm mouse line" (34).

References

1. Cooke, H. J., and Saunders, P. T. K. (2002) Mouse models of male infertility. *Nat. Rev. Genet.* **3,** 790–801
2. Dam, A. H. D. M., Feenstra, I., Westphal, J. R., Ramos, L., van Golde, R. J. T., and Kremer, J. A. M. (2007) Globozoospermia revisited. *Hum. Reprod. Update* **13,** 63–75
3. Okabe, M. (2013) The cell biology of mammalian fertilization. *Development* **140,** 4471–4479
4. Hunte, C., Screpanti, E., Venturi, M., Rimon, A., Padan, E., and Michel, H. (2005) Structure of a Na^+/H^+ antiporter and insights into mechanism of action and regulation by pH. *Nature* **435,** 1197–1202
5. Orlowski, J., and Grinstein, S. (2011) Na^+/H^+ exchangers. *Compr. Physiol.* **1,** 2083–2100
6. Schultheis, P. J., Clarke, L. L., Meneton, P., Miller, M. L., Soleimani, M., Gawenis, L. R., Riddle, T. M., Duffy, J. J., Doetschman, T., Wang, T., Giebisch, G., Aronson, P. S., Lorenz, J. N., and Shull, G. E. (1998) Renal and intestinal absorptive defects in mice lacking the NHE3 Na^+/H^+ exchanger. *Nat. Genet.* **19,** 282–285
7. Bell, S. M., Schreiner, C. M., Schultheis, P. J., Miller, M. L., Evans, R. L., Vorhees, C. V., Shull, G. E., and Scott, W. J. (1999) Targeted disruption of the murine Nhe1 locus induces ataxia, growth retardation, and seizures. *Am. J. Physiol. Cell Physiol.* **276,** C788–C795
8. Cox, G. A., Lutz, C. M., Yang, C. L., Biemesderfer, D., Bronson, R. T., Fu, A., Aronson, P. S., Noebels, J. L., and Frankel, W. N. (1997) Sodium/hydrogen exchanger gene defect in slow-wave epilepsy mutant mice. *Cell* **91,** 139–148
9. Bourgeois, S., Meer, L. V., Wootla, B., Bloch-Faure, M., Chambrey, R., Shull, G. E., Gawenis, L. R., and Houillier, P. (2010) NHE4 is critical for the renal handling of ammonia in rodents. *J. Clin. Invest.* **120,** 1895–1904
10. Rivinoja, A., Hassinen, A., Kokkonen, N., Kauppila, A., and Kellokumpu, S. (2009) Elevated Golgi pH impairs terminal *N*-glycosylation by inducing mislocalization of Golgi glycosyltransferases. *J. Cell. Physiol.* **220,** 144–154
11. Huang, C., and Chang, A. (2011) pH-dependent cargo sorting from the Golgi. *J. Biol. Chem.* **286,** 10058–10065
12. Orlowski, J., and Grinstein, S. (2007) Emerging roles of alkali cation/proton exchangers in organellar homeostasis. *Curr. Opin. Cell Biol.* **19,** 483–492
13. Forgac, M. (2007) Vacuolar ATPases: rotary proton pumps in physiology and pathophysiology. *Nat. Rev. Mol. Cell Biol.* **8,** 917–929
14. Ouyang, Q., Lizarraga, S. B., Schmidt, M., Yang, U., Gong, J., Ellisor, D., Kauer, J. A., and Morrow, E. M. (2013) Christianson syndrome protein NHE6 modulates TrkB endosomal signaling required for neuronal circuit development. *Neuron* **80,** 97–112
15. Kondapalli, K. C., Hack, A., Schushan, M., Landau, M., Ben-Tal, N., and Rao, R. (2013) Functional evaluation of autism-associated mutations in NHE9. *Nat. Commun.* **4,** 2510
16. Brett, C. L., Tukaye, D. N., Mukherjee, S., and Rao, R. (2005) The yeast endosomal $Na^+(K^+)/H^+$ exchanger Nhx1 regulates cellular pH to control vesicle trafficking. *Mol. Biol. Cell.* **16,** 1396–1405
17. Nakamura, N., Tanaka, S., Teko, Y., Mitsui, K., and Kanazawa, H. (2005) Four Na^+/H^+ exchanger isoforms are distributed to Golgi and post-Golgi compartments and are involved in organelle pH regulation. *J. Biol. Chem.* **280,** 1561–1572
18. Roxrud, I., Raiborg, C., Gilfillan, G. D., Strømme, P., and Stenmark, H. (2009) Dual degradation mechanisms ensure disposal of NHE6 mutant protein associated with neurological disease. *Exp. Cell Res.* **315,** 3014–3027
19. Xinhan, L., Matsushita, M., Numaza, M., Taguchi, A., Mitsui, K., and Kanazawa, H. (2011) Na^+/H^+ exchanger isoform 6 (NHE6/SLC9A6) is involved in clathrin-dependent endocytosis of transferrin. *Am. J. Physiol. Cell Physiol.* **301,** C1431–C1444
20. Gilfillan, G. D., Selmer, K. K., Roxrud, I., Smith, R., Kyllerman, M., Eiklid, K., Kroken, M., Mattingsdal, M., Egeland, T., Stenmark, H., Sjøholm, H., Server, A., Samuelsson, L., Christianson, A., Tarpey, P., et al. (2008) *SLC9A6* mutations cause X-linked mental retardation, microcephaly, epilepsy, and ataxia, a phenotype mimicking Angelman syndrome. *Am. J. Hum. Genet.* **82,** 1003–1010
21. Morrow, E. M., Yoo, S.-Y., Flavell, S. W., Kim, T.-K., Lin, Y., Hill, R. S., Mukaddes, N. M., Balkhy, S., Gascon, G., Hashmi, A., Al-Saad, S.,

Ware, J., Joseph, R. M., Greenblatt, R., Gleason, D., Ertelt, J. A., Apse, K. A., Bodell, A., Partlow, J. N., Barry, B., Yao, H., et al. (2008) Identifying autism loci and genes by tracing recent shared ancestry. *Science.* **321,** 218–223

22. Goyal, S., Vanden Heuvel, G., and Aronson, P. S. (2003) Renal expression of novel Na^+/H^+ exchanger isoform NHE8. *Am. J. Physiol. Renal Physiol.* **284,** F467–F473
23. Lawrence, S. P., Bright, N. A., Luzio, J. P., and Bowers, K. (2010) The sodium/proton exchanger NHE8 regulates late endosomal morphology and function. *Mol. Biol. Cell* **21,** 3540–3551
24. Xu, H., Chen, R., and Ghishan, F. K. (2005) Subcloning, localization, and expression of the rat intestinal sodium-hydrogen exchanger isoform 8. *Am. J. Physiol. Gastrointest. Liver Physiol.* **289,** G36–G41
25. Goyal, S., Mentone, S., and Aronson, P. S. (2005) Immunolocalization of NHE8 in rat kidney. *Am. J. Physiol. Renal Physiol.* **288,** F530–F538
26. Xu, H., Zhang, B., Li, J., Wang, C., Chen, H., and Ghishan, F. K. (2012) Impaired mucin synthesis and bicarbonate secretion in the colon of NHE8 knockout mice. *Am. J. Physiol. Gastrointest. Liver Physiol.* **303,** G335–G343
27. Liu, C., Xu, H., Zhang, B., Johansson, M. E. V., Li, J., Hansson, G. C., and Ghishan, F. K. (2013) NHE8 plays an important role in mucosal protection via its effect on bacterial adhesion. *Am. J. Physiol. Cell Physiol.* **305,** C121–C128
28. Jadeja, S., Barnard, A. R., McKie, L., Cross, S. H., White, J. K.; on behalf of the Sanger Mouse Genetics Project; Robertson, M., Budd, P. S., MacLaren, R. E., and Jackson, I. J. (2015) Mouse *Slc9a8* mutants exhibit retinal defects due to retinal pigmented epithelium dysfunction. *Invest. Ophthalmol. Vis. Sci.* **56,** 3015–3026
29. Xia, C.-H., Liu, H., Cheung, D., Tang, F., Chang, B., Li, M., and Gong, X. (2015) NHE8 is essential for RPE cell polarity and photoreceptor survival. *Sci. Rep.* **5,** 9358
30. Xu, H., Chen, H., Li, J., Zhao, Y., and Ghishan, F. K. (2015) Disruption of NHE8 expression impairs Leydig cell function in the testes. *Am. J. Physiol. Cell Physiol.* **308,** C330–C338
31. Zhou, Q., Clarke, L., Nie, R., Carnes, K., Lai, L. W., Lien, Y. H., Verkman, A., Lubahn, D., Fisher, J. S., Katzenellenbogen, B. S., and Hess, R. A. (2001) Estrogen action and male fertility: roles of the sodium/hydrogen exchanger-3 and fluid reabsorption in reproductive tract function. *Proc. Natl. Acad. Sci. U.S.A.* **98,** 14132–14137
32. Wang, D., King, S. M., Quill, T. A., Doolittle, L. K., and Garbers, D. L. (2003) A new sperm-specific Na^+/H^+ exchanger required for sperm motility and fertility. *Nat. Cell Biol.* **5,** 1117–1122
33. Wang, D., Hu, J., Bobulescu, I. A., Quill, T. A., McLeroy, P., Moe, O. W., and Garbers, D. L. (2007) A sperm-specific Na^+/H^+ exchanger (sNHE) is critical for expression and *in vivo* bicarbonate regulation of the soluble adenylyl cyclase (sAC). *Proc. Natl. Acad. Sci. U.S.A.* **104,** 9325–9330
34. Hasuwa, H., Muro, Y., Ikawa, M., Kato, N., Tsujimoto, Y., and Okabe, M. (2010) Transgenic mouse sperm that have green acrosome and red mitochondria allow visualization of sperm and their acrosome reaction *in vivo*. *Exp. Anim.* **59,** 105–107
35. Mortimer, D., Curtis, E. F., and Miller, R. G. (1987) Specific labelling by peanut agglutinin of the outer acrosomal membrane of the human spermatozoon. *J. Reprod. Fertil.* **81,** 127–135
36. Ramalho-Santos, J., Varum, S., Amaral, S., Mota, P. C., Sousa, A. P., and Amaral, A. (2009) Mitochondrial functionality in reproduction: from gonads and gametes to embryos and embryonic stem cells. *Hum. Reprod. Update* **15,** 553–572
37. Zhang, F. P., Poutanen, M., Wilbertz, J., and Huhtaniemi, I. (2001) Normal prenatal but arrested postnatal sexual development of luteinizing hormone receptor knockout (LuRKO) mice. *Mol. Endocrinol.* **15,** 172–183
38. Kierszenbaum, A. L., Rivkin, E., and Tres, L. L. (2003) Acroplaxome, an F-actin-keratin-containing plate, anchors the acrosome to the nucleus during shaping of the spermatid head. *Mol. Biol. Cell* **14,** 4628–4640
39. Lécureuil, C., Fontaine, I., Crepieux, P., and Guillou, F. (2002) Sertoli and granulosa cell-specific Cre recombinase activity in transgenic mice. *Genesis* **33,** 114–118
40. Sadate-Ngatchou, P. I., Payne, C. J., Dearth, A. T., and Braun, R. E. (2008) Cre recombinase activity specific to postnatal, premeiotic male germ cells in transgenic mice. *Genesis* **46,** 738–742
41. Soriano, P. (1999) Generalized lacZ expression with the ROSA26 Cre reporter strain. *Nat. Genet.* **21,** 70–71
42. Holstein, A. F., Schirren, C. G., Schirren, C., and Mauss, J. (1973) [Round headed spermatozoa: a cause of male infertility]. *Dtsch. Med. Wochenschr.* **98,** 61–62
43. Shirren Sen, C. G., Holstein, A. F., and Schirren, C. (1971) On the morphogenesis of roundheaded spermatozoa of human. *Andrologia.* **3,** 117–125
44. Scott, C. C., and Gruenberg, J. (2011) Ion flux and the function of endosomes and lysosomes: pH is just the start: the flux of ions across endosomal membranes influences endosome function not only through regulation of the luminal pH. *BioEssays* **33,** 103–110
45. Berruti, G. (2016) Towards defining an "origin"–The case for the mammalian acrosome. *Semin. Cell Dev. Biol.* **59,** 46–53
46. Inoue, N., Ikawa, M., Isotani, A., and Okabe, M. (2005) The immunoglobulin superfamily protein Izumo is required for sperm to fuse with eggs. *Nature.* **434,** 234–238
47. Yao, R., Ito, C., Natsume, Y., Sugitani, Y., Yamanaka, H., Kuretake, S., Yanagida, K., Sato, A., Toshimori, K., and Noda, T. (2002) Lack of acrosome formation in mice lacking a Golgi protein, GOPC. *Proc. Natl. Acad. Sci. U.S.A.* **99,** 11211–11216
48. Kang-Decker, N., Mantchev, G. T., Juneja, S. C., McNiven, M. A., and van Deursen, J. M. (2001) Lack of acrosome formation in Hrb-deficient mice. *Science.* **294,** 1531–1533
49. Xiao, N., Kam, C., Shen, C., Jin, W., Wang, J., Lee, K. M., Jiang, L., and Xia, J. (2009) PICK1 deficiency causes male infertility in mice by disrupting acrosome formation. *J. Clin. Invest.* **119,** 802–812
50. Moreno, R. D., and Alvarado, C. P. (2006) The mammalian acrosome as a secretory lysosome: new and old evidence. *Mol. Reprod. Dev.* **73,** 1430–1434
51. Berruti, G., and Paiardi, C. (2011) Acrosome biogenesis: revisiting old questions to yield new insights. *Spermatogenesis* **1,** 95–98
52. Qiu, Q.-S., and Fratti, R. A. (2010) The Na^+/H^+ exchanger Nhx1p regulates the initiation of *Saccharomyces cerevisiae* vacuole fusion. *J. Cell Sci.* **123,** 3266–3275
53. Cheng, X., Shen, D., Samie, M., and Xu, H. (2010) Mucolipins: intracellular TRPML1–3 channels. *FEBS Lett.* **584,** 2013–2021
54. Arndt, L., Castonguay, J., Arlt, E., Meyer, D., Hassan, S., Borth, H., Zierler, S., Wennemuth, G., Breit, A., Biel, M., Wahl-Schott, C., Gudermann, T., Klugbauer, N., and Boekhoff, I. (2014) NAADP and the two-pore channel protein 1 participate in the acrosome reaction in mammalian spermatozoa. *Mol. Biol. Cell* **25,** 948–964
55. Luzio, J. P., Bright, N. A., and Pryor, P. R. (2007) The role of calcium and other ions in sorting and delivery in the late endocytic pathway. *Biochem. Soc. Trans.* **35,** 1088–1091
56. Meizel, S., and Deamer, D. W. (1978) The pH of the hamster sperm acrosome. *J. Histochem. Cytochem.* **26,** 98–105
57. Nakanishi, T., Ikawa, M., Yamada, S., Toshimori, K., and Okabe, M. (2001) Alkalinization of acrosome measured by GFP as a pH indicator and its relation to sperm capacitation. *Dev. Biol.* **237,** 222–231
58. Modi, S., Nizak, C., Surana, S., Halder, S., and Krishnan, Y. (2013) Two DNA nanomachines map pH changes along intersecting endocytic pathways inside the same cell. *Nat. Nanotechnol.* **8,** 459–467
59. Condon, K. H., Ho, J., Robinson, C. G., Hanus, C., and Ehlers, M. D. (2013) The Angelman syndrome protein Ube3a/E6AP is required for Golgi acidification and surface protein sialylation. *J. Neurosci.* **33,** 3799–3814
60. Maeda, Y., Ide, T., Koike, M., Uchiyama, Y., and Kinoshita, T. (2008) GPHR is a novel anion channel critical for acidification and functions of the Golgi apparatus. *Nat. Cell Biol.* **10,** 1135–1145
61. Marshansky, V., and Futai, M. (2008) The V-type H^+-ATPase in vesicular trafficking: targeting, regulation and function. *Curr. Opin. Cell Biol.* **20,** 415–426
62. Clague, M. J., Urbé, S., Aniento, F., and Gruenberg, J. (1994) Vacuolar ATPase activity is required for endosomal carrier vesicle formation. *J. Biol. Chem.* **269,** 21–24
63. Hurtado-Lorenzo, A., Skinner, M., El Annan, J., Futai, M., Sun-Wada, G.-H., Bourgoin, S., Casanova, J., Wildeman, A., Bechoua, S., Ausiello, D. A., Brown, D., and Marshansky, V. (2006) V-ATPase interacts with ARNO and Arf6 in early endosomes and regulates the protein degradative pathway. *Nat. Cell Biol.* **8,** 124–136

64. Liu, G., Shi, Q.-W., and Lu, G.-X. (2010) A newly discovered mutation in PICK1 in a human with globozoospermia. *Asian J. Androl.* **12,** 556–560
65. Koscinski, I., Elinati, E., Fossard, C., Redin, C., Muller, J., Velez de la Calle, J., Schmitt, F., Ben Khelifa, M., Ray, P. F., Ray, P., Kilani, Z., Barratt, C. L. R., and Viville, S. (2011) DPY19L2 deletion as a major cause of globozoospermia. *Am. J. Hum. Genet.* **88,** 344–350
66. Dam, A. H. D. M., Koscinski, I., Kremer, J. A. M., Moutou, C., Jaeger, A.-S., Oudakker, A. R., Tournaye, H., Charlet, N., Lagier-Tourenne, C., van Bokhoven, H., and Viville, S. (2007) Homozygous mutation in SPATA16 is associated with male infertility in human globozoospermia. *Am. J. Hum. Genet.* **81,** 813–820
67. Schwenk, F., Baron, U., and Rajewsky, K. (1995) A cre-transgenic mouse strain for the ubiquitous deletion of loxP-flanked gene segments including deletion in germ cells. *Nucleic Acids Res.* **23,** 5080–5081
68. Farley, F. W., Soriano, P., Steffen, L. S., and Dymecki, S. M. (2000) Widespread recombinase expression using FLPeR (flipper) mice. *Genesis* **28,** 106–110

Loss of the Na^+/H^+ exchanger NHE8 causes male infertility in mice by disrupting acrosome formation

Karina Oberheide, Dmytro Puchkov and Thomas J. Jentsch

J. Biol. Chem. 2017, 292:10845-10854.
doi: 10.1074/jbc.M117.784108 originally published online May 5, 2017